Amplification of Dissymmetry Factors in π-Extended [7]- and [9]Helicenes

Article

Amplification of Dissymmetry Factors in π-Extended [7]- and [9]Helicenes

Zijie Qiu, Cheng-Wei Ju, Lucas Frédéric, Yunbin Hu, Dieter Schollmeyer, Grégory Pieters,* Klaus Müllen,* and Akimitsu Narita*

Read Online

ACCESS | Metrics & More | Article Recommendations | Supporting Information

ABSTRACT: π-Extended helicenes constitute an important class of polycyclic aromatic hydrocarbons with intrinsic chirality. Herein, we report the syntheses of π-extended [7]helicene **4** and π-extended [9]helicene **6** through regioselective cyclodehydrogenation in high yields, where a "prefusion" strategy plays a key role in preventing undesirable aryl rearrangements. The unique helical structures are unambiguously confirmed by X-ray crystal structure analysis. Compared to the parent pristine [7]helicene and [9]helicene, these novel π-extended helicenes display significantly improved photophysical properties, with a quantum yield of 0.41 for **6**.

After optical resolution by chiral high-performance liquid chromatography, the chiroptical properties of enantiomers **4**-*P/M* and **6**-*P/M* are investigated, revealing that the small variation in helical length from [7] to [9] can cause an approximately 10-fold increase in the dissymmetry factors. The circularly polarized luminescence brightness of **6** reaches 12.6 M^{-1} cm^{-1} as one of the highest among carbohelicenes.
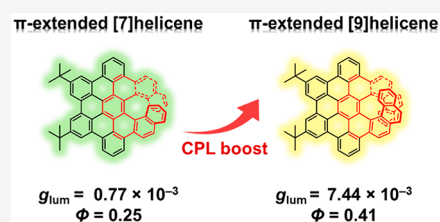
INTRODUCTION

Carbohelicenes constitute a unique class of polycyclic aromatic hydrocarbons with benzene rings that are angularly annulated in the *ortho*-configuration. The helical structures lead to intrinsic chirality and allow applications in asymmetric catalysis, nonlinear optics, and molecular machines.[1,2] Theoretical studies have shown that the dissymmetry factor (g) of single-stranded [n]carbohelicenes increases with the helical length n.[3] Therefore, tremendous efforts have been made to synthesize higher [n]helicenes since the first report of [6]helicene by Newman and Lednicer in 1956.[4−7] To date, the longest carbohelicene reported is [16]helicene, which was synthesized by Fujita and co-workers in 2015.[8] The low yield of the final photocyclization step (7%), however, hinders a further increase of the helical length by this approach.

Another research direction in helicene chemistry is the lateral extension of π-conjugated systems.[9−20] With more extensive conjugation, π-extended helicenes can be regarded as nanosolenoids and are predicted to possess intriguing electronic, magnetic, and spin properties.[21−23] In addition, their fascinating chiroptical features, such as circular dichroism (CD) and circularly polarized luminescence (CPL), have been intensively studied and are valuable for circularly polarized organic light-emitting diodes and bioimaging applications.[24−27]

An ideal CPL emitter should possess both a high emission quantum yield (Φ) and a large luminescence dissymmetry factor (g_{lum}), but these properties are often difficult to achieve simultaneously. One rare cylindrical molecule with D_4 symmetry was reported to possess a Φ of 0.80 and an exceptional $|g_{lum}|$ of 0.152 by Isobe et al.[28] Hexa-*peri*-hexabenzocoronene (HBC) and perylene diimide (PDI) have been commonly used as the skeletons for π-extension. However, the potential of such π-extended helicenes as CPL emitters has not been well explored. For example, an excellent Φ (>0.80) was achieved by a HBC-fused oxa[7]superhelicene, but its g_{lum} was only 2×10^{-4} (Scheme 1A);[10,29] a moderate g_{lum} (2×10^{-3}) and a low Φ (0.098) were reported for another HBC-based undecabenzo[7]superhelicene (Scheme 1B);[9,23] and in a series of PDI-embedding double [8]helicenes, only moderate values of g_{lum} (up to 2×10^{-3}) and Φ (up to 0.30) were observed (Scheme 1C).[19] After the initial submission of

Scheme 1. π-Extended Helicenes and Their CPL Properties
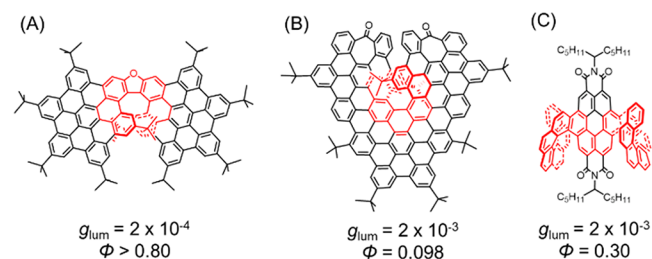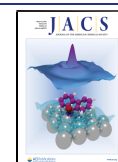
this manuscript, Santoro, Schuster, Nuckolls et al. reported amplified CD signals by extending the helical length, but did not study the CPL performance.[27] Therefore, the design and synthesis of π-extended helicenes with a good balance between fluorescence performance and dissymmetry factors are highly desired.

In this study, we targeted a series of π-extended [n]helicenes with various helical lengths n. The tribenzo[fg,ij,rst]-pentaphene, a segment of HBC, is selected as the π-extension motif, which is expected to inherit the merits of HBC in terms of optoelectronic and photophysical properties.[30] In our first attempt to synthesize π-extended [7]helicene **4** from precursor **1**, heptagon-bearing [5]helicene **2** was selectively obtained due to unexpected aryl rearrangement during cyclodehydrogenation (Scheme 2A).[31] Computational studies of the reaction

Scheme 2. Illustration of the Prefusion Strategy To Prevent Aryl Rearrangement and Achieve the Desired π-Extended Helicenes 4 and 6
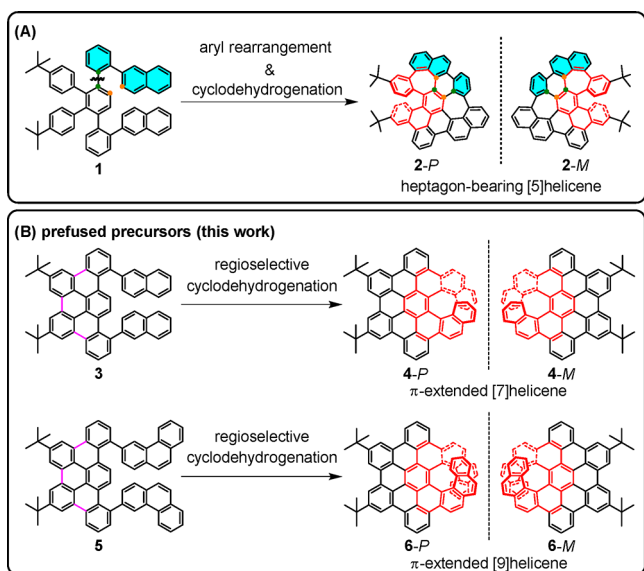
mechanism indicated that the rearrangement occurred in the first step of dehydrogenation and was favored over direct C—C bond formation for **4**. To prevent this undesired yet highly efficient aryl rearrangement, we herein adopted a new strategy that employs precursors **3** and **5** by prefusing the tetraphenyl-benzene moiety (Scheme 2B). Targeted π-extended helicenes **4** and **6** were thus successfully obtained by regioselective cyclodehydrogenation in high yields. The helical structures of **4** and **6** were confirmed by NMR spectroscopy and X-ray crystallography. Their high isomerization barriers (>40 kcal/mol) enabled the separation of enantiomers **4**-P/M and **6**-P/M by chiral high-performance liquid chromatography (HPLC). Intriguingly, the combination of the elongated helical length and extended π-conjugation empower **6** as a promising CPL emitter with a Φ_f of 0.41 and a g_{lum} of 7.4 × 10^{-3}, distinguishing it from π-extended carbohelicenes in the literature.

■ RESULTS AND DISCUSSION

As depicted in Figure 1A, the syntheses of π-extended helicenes **4** and **6** started from dibromo-functionalized 1,2,3,4-tetraphenyl benzene **7**, which was reported in a previous paper.[31] Compound **7** was treated with 2,3-

dichloro-5,6-dicyano-1,4-benzoquinone (DDQ) and trifluoro-methanesulfonic acid (TfOH) in dry dichloroethane at 30 °C under nitrogen to produce dibromo tribenzo[fg,ij,rst]-pentaphene **8** as the prefused building block in 49% yield. Compound **8** was then coupled to 2-naphthyl groups by the Suzuki reaction to yield precursor **3**. Compared to those in precursor **1**, the phenyl rings in **3** were fully fused and thus incorporated into the polycyclic lattice, leaving only the naphthyl groups for the subsequent Scholl reaction. The final cyclodehydrogenation using DDQ and TfOH proceeded regioselectively at 0 °C, affording the desired π-extended [7]helicene **4** as a yellow solid in 76% yield. Similarly, precursor **5** functionalized with phenanthryl units was synthesized from **8**. The subsequent regioselective cyclo-dehydrogenation of **5** resulted in π-extended [9]helicene **6** in a high yield of 84%. The regioselective cyclodehydrogenation of **3** and **5** could also be achieved in similar yields (72% and 79%, respectively) by using FeCl$_3$ as oxidant at room temperature, but no reaction was observed in oxidative photocyclization by iodine without heating. Notably, the conditions of highly regioselective Scholl reaction (DDQ/FeCl$_3$) of the phenanthr-yl units in this work are much milder than the previously reported oxidative photocyclization (100 °C for 24 h).[32]

The chemical structures of π-extended helicenes **4** and **6** were fully characterized by standard spectroscopic techniques. In high-resolution matrix-assisted laser desorption/ionization-time-of-flight mass spectrometry (MALDI-TOF MS), **4** and **6** displayed strong signals at m/z = 736.3110 and 836.3443, respectively, with isotopic distribution patterns consistent with the calculated spectra (Figures S8 and S16). With the aid of ¹H−¹H correlation spectroscopy measurements, all proton peaks of **4** and **6** in the aromatic region were assigned (Figure 1B and C). Notably, the proton signals corresponding to the end of the helices (peaks 9, 10, and 11 in **4**; peaks 11', 12', and 13' in **6**) exhibited pronounced upfield chemical shifts (δ = 5.57−7.00 ppm) due to the shielding effects induced by spatial overlap with other benzene rings.

Single crystals of precursor **3** as well as π-extended helicenes **4** and **6** were grown by slow diffusion of ethanol vapor into their chloroform solutions (Figures 2 and S17). The helical structures of **4** and **6** were thus confirmed by X-ray diffraction. Due to the rigidification provided by the tribenzo[fg,ij,rst]-pentaphene subunits, the torsion angles in the helices were similar, with values of 20.6° for **4**-M (atoms a−b−c−d) and 20.9° for **6**-M (atoms a'−b'−c'−d'), as depicted in Figure 2A and 2C. The helical pitch, which was determined from the centroid−centroid distance of the overlapping benzene rings (Figure 2B and 2D), was 3.95 and 3.54 Å in **4** and **6**, respectively. These lengths are slightly larger than the values for parent [7]helicene **9** (3.87 Å; CCDC: 852537) and [9]helicene **10** (3.52 Å; CCDC: 1051158) reported in the literature (the chemical structures of **9** and **10** are shown in Scheme S1).[8,33] P/M enantiomer pairs were identified in the molecular packing, where enantiomers with the same chirality (P or M) are packed in a columnar fashion in both **4** and **6** (Figure 2E and F). However, pronounced intermolecular π−π interactions were suppressed by the twisted helical sub-structure.

The absorption and emission spectra of **4** and **6** in THF solutions were investigated and exhibited similar shapes (Figures 3A and S18). The absorption maximum (λ_{abs}) of **4** was at 441 nm, and its emission peak (λ_{em}) was centered at 495 nm. Because of its increased helical length n, **6** possesses
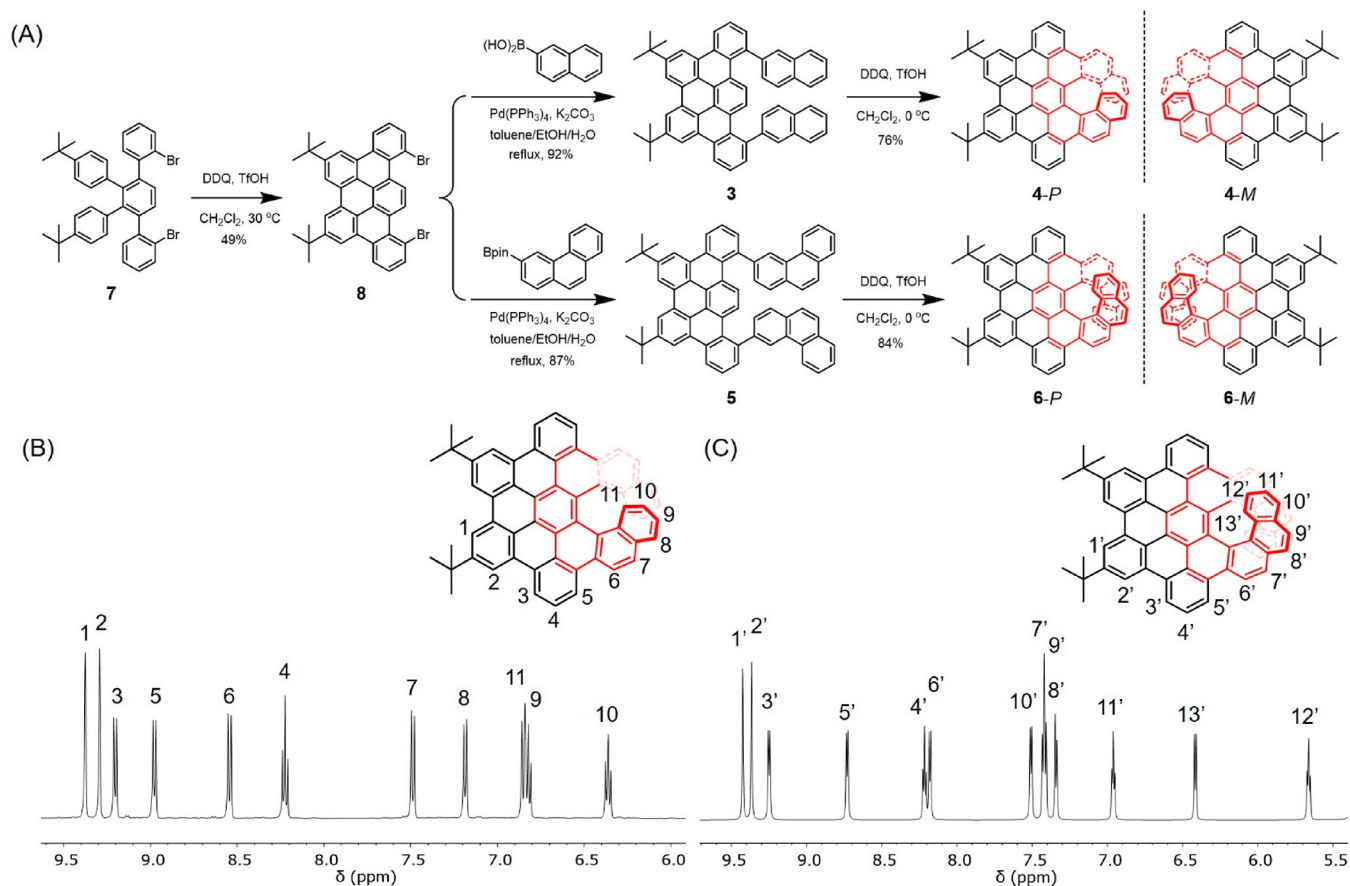
Figure 1. (A) Synthetic route toward **4** and **6**. (B and C) Aromatic regions of the ^{1}H NMR spectra of **4** and **6** with peak assignments.
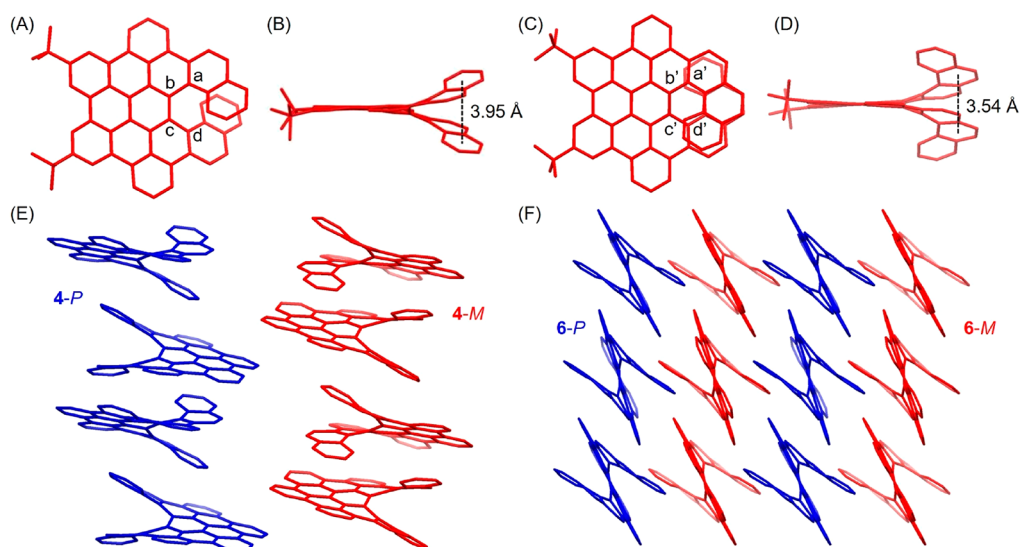

Figure 2. Single-crystal structures of (A and B) **4**-*M* and (C and D) **6**-*M*. (E and F) Molecular packing of **4** and **6**. All hydrogen atoms and the *tert*-butyl groups in (E and F) are omitted for clarity. The *P*- and *M*-enantiomers are highlighted in blue and red, respectively.

greater π-conjugation than **4**, as supported by its red-shifted absorption and emission bands (λ_{abs} = 452 nm and λ_{em} = 528 nm). Interestingly, **4** and **6** emitted strong greenish fluorescence with Φ of 0.25 and 0.41, respectively, whereas **9** and **10** displayed much lower values (<0.02).[34,35] This clearly demonstrates the added value of the π-extension in terms of photophysical properties. The transient PL spectra revealed an average lifetime of 16.2 ns for **4** and 8.8 ns for **6**, confirming

the prompt fluorescence nature of their emission (Figure S19). Since similar nonradiative rates (k_{nr}) were observed for **4** and **6** (4.6×10^7 s^{-1} and 6.8×10^7 s^{-1}, respectively), the higher fluorescence Φ of **6** can be attributed to the increase in the radiative rate constant ($k_r = 1.5 \times 10^7$ s^{-1} for **4** and $k_r = 4.5 \times 10^7$ s^{-1} for **6**). In addition, these π-extended helicenes were also emissive in the solid state (Φ = 0.17 and 0.34 for **4** and **6**, respectively) with red-shifted bands (Figure S18) as a result of
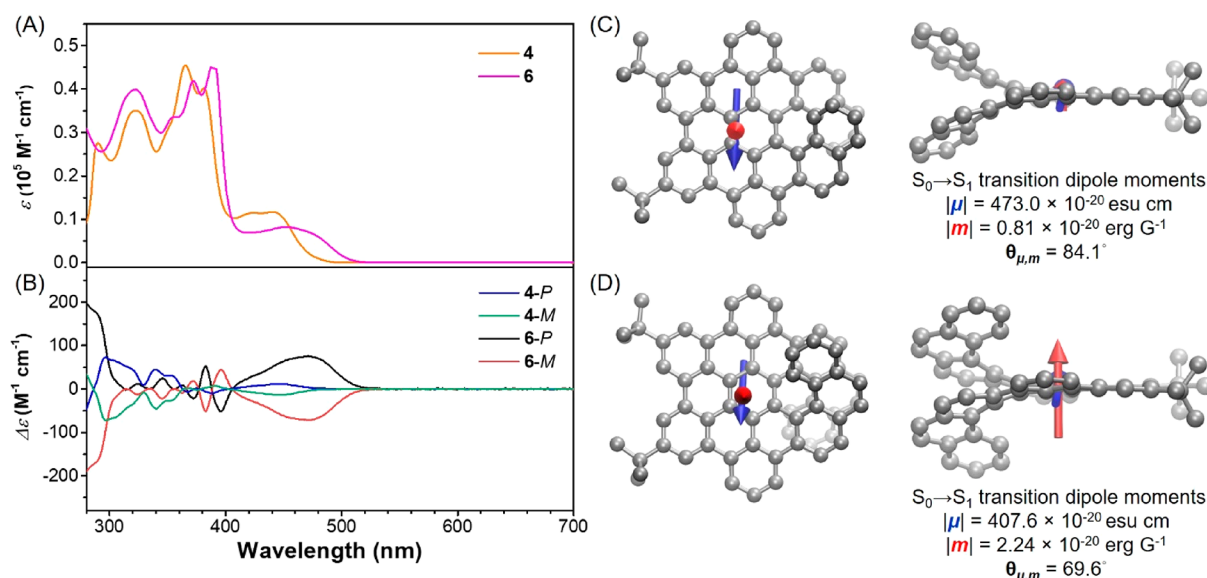
Figure 3. (A) Absorption spectra and (B) CD spectra of **4** and **6** in THF solutions. Solution concentration: 10^{-5} M. (C and D) Transition dipole moments of (C) **4-P** and (D) **6-P** for the $S_0 \rightarrow S_1$ transition. The electric transition dipole moments (μ) are shown in blue, and the magnetic transition dipole moments (m) are shown in red. The length of the m vector is amplified 200 times for clarity.

Table 1. Summary of the Chiroptical Properties of 4-P and 6-P

	CD^a				$S_0 \rightarrow S_1$ transition^b				CPL^a		
	λ (nm)	$\Delta\varepsilon$ (M^{-1} cm^{-1})	E (M^{-1} cm^{-1})	g_{abs} (10^{-3})	$|\mu|$ (10^{-20} esu cm)	$|m|$ (10^{-20} erg G^{-1})	θ (deg)	g_{cal} (10^{-3})	λ_{em} (nm)	g_{lum} (10^{-3})	B_{CPL} (M^{-1} cm^{-1})
4-P	446	13.9	11 255	1.24	469.2	0.81	84.1	0.71	486	0.77	1.1
6-P	471	75.2	7108	10.58	407.0	2.24	69.6	7.60	532	7.44	12.6

^{a}Measured in a dilute THF solution. Concentration: 10^{-5} M. ^{b}Calculated by TD-DFT at the B3LYP/6-311G (d,p) level.

their nonplanar structures and thus suppressed intermolecular $\pi-\pi$ stacking. By means of time-dependent density functional theory (TD-DFT) calculations, the first absorption peaks of **4** and **6** were assigned to the HOMO → LOMO transitions (H → L), where the electron cloud was distributed throughout the whole molecule (Figure S22). The photophysical properties and calculated major transitions of **4** and **6** are summarized in Tables S1−S3.

To investigate the *P/M* racemization barriers of **4** and **6**, DFT calculations were performed to identify the transition states with the highest Gibbs free energy, in which the terminal benzene rings in the helix were oriented in a face-to-face pattern (Figure S24). Accordingly, the *P/M* isomerization barriers of **4** and **6** were calculated to be 42.4 and 41.6 kcal/mol, respectively. These values are close to those reported for **9** and **10**,[36] indicating that π-extension barely affected the rigidity of the helical backbones. Such high *P/M* isomerization barriers are marked by the high thermal stability of their enantiomers. No racemization was observed when the solutions of **4-M** and **6-M** were heated at 150 °C for 60 min (Figure S21).

Due to the high isomerization barriers, the enantiomers of **4** and **6** could be completely resolved by HPLC with a Daicel Chiralpak IE column (Figure S20). The CD spectra of isolated enantiomers **4-P/M** and **6-P/M** in THF solutions (10^{-5} M) were measured. Upon comparing the experimental and DFT-simulated CD spectra, the absolute configurations in the first and second fractions of the chiral HPLC analysis were assigned as the *P*- and *M*-enantiomers, respectively, for both **4** and **6**. Interestingly, because of the increase in the helical length *n* from 7 to 9, π-extended [9]helicene **6** exhibited a much higher

$\Delta\varepsilon$ than **4** in the long-wavelength region (Figure 3B). From the UV−vis spectra, the absorption dissymmetry factors ($g_{abs} = \Delta\varepsilon/\varepsilon$)[37] of **4-P** and **6-P** at their absorption maximum peaks were calculated to be 1.24×10^{-3} and 10.58×10^{-3}, respectively (Table 1). The dramatically higher value of g_{abs} for **6** was also supported by the simulated CD spectra (Figure S23A). For comparison, the CD spectra of non-π-extended helicenes **9** and **10** were also simulated by TD-DFT at the same level of theory. Unlike those of π-extended helicenes **4** and **6**, the CD signal intensities of **9** and **10** were not substantially affected by increasing the helical length *n* (Figure S23B).[3] According to the absorption peak assignment discussed above, the first peak in the CD spectra originates from the chirality of the whole molecule for both **4** and **6**. Consequently, the drastic changes in the dissymmetry factors of our π-extended helicenes result from the combined effect of lateral and helical extensions.

According to theory, g_{abs} can be determined by the following equation:

$$g_{abs} = 4 \cos\theta \frac{|\mu||m|}{|\mu|^2 + |m|^2}$$

Therefore, the electronic (μ) and magnetic (m) transition dipole moments, as well as the angle (θ) between μ and m, of **4-P** and **6-P** for their $S_0 \rightarrow S_1$ transitions were determined by means of TD-DFT calculations (Table 1). For organic materials, the $|m|$ value is normally much lower than the $|\mu|$ value. The above equation can thus be simplified as $g_{abs} = 4 \cos\theta \, |m|/|\mu|$. The higher $|m|$, lower $|\mu|$, and larger $\cos\theta$ of **6** than of **4** all lead to an increase in the calculated absorption

dissymmetry factor (g_{cal}) by a factor of 10 with respect to that of **4**, consistent with the trend observed experimentally.

Subsequently, the CPL spectra of **4**-*P/M* and **6**-*P/M* were also measured to explore the potential of these compounds as chiral emitters.[37] Mirror images of the CPL spectra and g_{lum} plots were observed for the *P*- and *M*-enantiomers of both **4** and **6** (Figure 4). Similar to the CD properties, the CPL
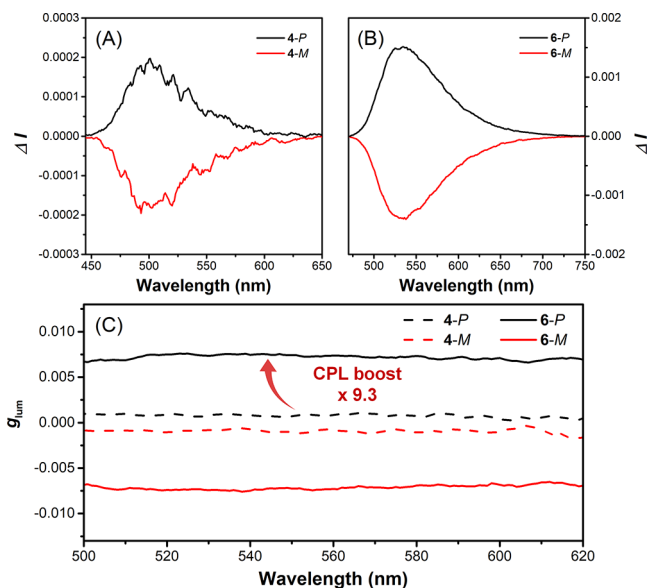

Figure 4. (A and B) CPL emission spectra and (C) luminescence dissymmetry factors of **4**-*P/M* and **6**-*P/M* in THF. Concentration: 10^{-5} M. Excitation: 380 nm for **4** and 425 nm for **6**.

intensity (ΔI) and g_{lum} of **6** were significantly enhanced ($g_{lum, 6\text{-}P}$ = 7.4 × 10^{-3}) with a high signal-to-noise ratio. Following the concept of fluorescence brightness, the CPL brightness (B_{CPL}) has recently been proposed to evaluate the overall performance of CPL emitters:[38]

$$B_{CPL} = \varepsilon \times \Phi_f \times \frac{g_{lum}}{2}$$

With all the necessary chiroptical results in hand, the B_{CPL} of **6** was calculated to be 12.6 M^{-1} cm^{-1}, which is one of the highest values among all carbohelicenes reported in the literature,[38] indicating that **6** may be an excellent emitter for CPL applications.

CONCLUSION

In summary, two π-extended helicenes, **4** and **6**, were synthesized through regioselective cyclodehydrogenation in high yields. The design of prefused precursors **3** and **5** plays a key role in preventing undesirable aryl rearrangements. Studies of the chiroptical properties of these compounds have revealed the beneficial effect of their π-extension and helical subunits on their dissymmetry factors. Approximately 10-fold enhancements in g_{abs}, g_{lum}, and B_{CPL} were observed from **4** to **6**, indicating that **6** is a promising CPL emitter. More importantly, **4** and **6** can be used as model compounds for other π-extended helicenes with even higher helical lengths currently under investigation in our laboratory following the polymerization–cyclodehydrogenation approach. Because of both extended π-conjugation and stable chirality, this series of

π-extended helicenes are expected to possess high potential for spin transport[39−41] and superior inductance.[21]

ASSOCIATED CONTENT

Supporting Information

The Supporting Information is available free of charge at https://pubs.acs.org/doi/10.1021/jacs.0c13197.

Experimental details, characterization spectra of all synthesized compounds, single-crystal data, photophysical measurements, and computational details (PDF)

Accession Codes

CCDC 2047540−2047542 contain the supplementary crystallographic data for this paper. These data can be obtained free of charge via www.ccdc.cam.ac.uk/data_request/cif, or by emailing data_request@ccdc.cam.ac.uk, or by contacting The Cambridge Crystallographic Data Centre, 12 Union Road, Cambridge CB2 1EZ, UK; fax: +44 1223 336033.

AUTHOR INFORMATION

Corresponding Authors

Grégory Pieters − *Université Paris-Saclay, CEA, INRAE, Département Médicaments et Technologies pour la Santé (DMTS), SCBM, F-91191 Gif-sur-Yvette, France;* orcid.org/0000-0002-3924-8287; Email: gregory.pieters@cea.fr

Klaus Müllen − *Max Planck Institute for Polymer Research, 55128 Mainz, Germany; Department of Chemistry, University of Cologne, 50939 Cologne, Germany;* orcid.org/0000-0001-6630-8786; Email: muellen@mpip-mainz.mpg.de

Akimitsu Narita − *Max Planck Institute for Polymer Research, 55128 Mainz, Germany; Organic and Carbon Nanomaterials Unit, Okinawa Institute of Science and Technology Graduate University, Kunigami-gun, Okinawa 904-0495, Japan;* Email: akimitsu.narita@oist.jp

Authors

Zijie Qiu − *Max Planck Institute for Polymer Research, 55128 Mainz, Germany;* orcid.org/0000-0003-0728-1178

Cheng-Wei Ju − *Max Planck Institute for Polymer Research, 55128 Mainz, Germany;* orcid.org/0000-0002-2250-8548

Lucas Frédéric − *Université Paris-Saclay, CEA, INRAE, Département Médicaments et Technologies pour la Santé (DMTS), SCBM, F-91191 Gif-sur-Yvette, France*

Yunbin Hu − *Max Planck Institute for Polymer Research, 55128 Mainz, Germany; Department of Organic and Polymer Chemistry, College of Chemistry and Chemical Engineering, Central South University, Changsha, Hunan 410083, People's Republic of China;* orcid.org/0000-0001-5346-7059

Dieter Schollmeyer − *Institute of Organic Chemistry, Johannes Gutenberg-University Mainz, 55099 Mainz, Germany*

Complete contact information is available at:
https://pubs.acs.org/10.1021/jacs.0c13197

Notes

The authors declare no competing financial interest.

REFERENCES

(1) Gingras, M. One hundred years of helicene chemistry. Part 3: applications and properties of carbohelicenes. *Chem. Soc. Rev.* **2013**, *42*, 1051−1095.

(2) Shen, Y.; Chen, C. F. Helicenes: synthesis and applications. *Chem. Rev.* **2012**, *112*, 1463−1535.

(3) Nakai, Y.; Mori, T.; Inoue, Y. Theoretical and experimental studies on circular dichroism of carbo[n]helicenes. *J. Phys. Chem. A* **2012**, *116*, 7372−7385.

(4) Newman, M. S.; Lednicer, D. The Synthesis and Resolution of Hexahelicene. *J. Am. Chem. Soc.* **1956**, *78*, 4765−4770.

(5) Martin, R. H.; Morren, G.; Schurter, J. J. [13]Helicene and [13]helicene-10,21-d2. *Tetrahedron Lett.* **1969**, *10*, 3683−3688.

(6) Martin, R. H.; Baes, M. Helicenes: Photosyntheses of [11], [12] and [14]helicene. *Tetrahedron* **1975**, *31*, 2135.

(7) Jancarik, A.; Rybacek, J.; Cocq, K.; Vacek Chocholousova, J.; Vacek, J.; Pohl, R.; Bednarova, L.; Fiedler, P.; Cisarova, I.; Stara, I. G.; Stary, I. Rapid access to dibenzohelicenes and their functionalized derivatives. *Angew. Chem., Int. Ed.* **2013**, *52*, 9970−9975.

(8) Mori, K.; Murase, T.; Fujita, M. One-step synthesis of [16]helicene. *Angew. Chem., Int. Ed.* **2015**, *54*, 6847−6851.

(9) Cruz, C. M.; Castro-Fernandez, S.; Macoas, E.; Cuerva, J. M.; Campana, A. G. Undecabenzo[7]superhelicene: A Helical Nanographene Ribbon as a Circularly Polarized Luminescence Emitter. *Angew. Chem., Int. Ed.* **2018**, *57*, 14782−14786.

(10) Reger, D.; Haines, P.; Heinemann, F. W.; Guldi, D. M.; Jux, N. Oxa[7]superhelicene: A pi-Extended Helical Chromophore Based on Hexa-peri-hexabenzocoronenes. *Angew. Chem., Int. Ed.* **2018**, *57*, 5938−5942.

(11) Zhu, Y.; Xia, Z.; Cai, Z.; Yuan, Z.; Jiang, N.; Li, T.; Wang, Y.; Guo, X.; Li, Z.; Ma, S.; Zhong, D.; Li, Y.; Wang, J. Synthesis and Characterization of Hexapole [7]Helicene, A Circularly Twisted Chiral Nanographene. *J. Am. Chem. Soc.* **2018**, *140*, 4222−4226.

(12) Evans, P. J.; Ouyang, J.; Favereau, L.; Crassous, J.; Fernandez, I.; Perles, J.; Martin, N. Synthesis of a Helical Bilayer Nanographene. *Angew. Chem., Int. Ed.* **2018**, *57*, 6774−6779.

(13) Nakakuki, Y.; Hirose, T.; Sotome, H.; Miyasaka, H.; Matsuda, K. Hexa- peri-hexabenzo[7]helicene: Homogeneously pi-Extended Helicene as a Primary Substructure of Helically Twisted Chiral Graphenes. *J. Am. Chem. Soc.* **2018**, *140*, 4317−4326.

(14) Fujikawa, T.; Segawa, Y.; Itami, K. Synthesis, Structures, and Properties of pi-Extended Double Helicene: A Combination of Planar and Nonplanar pi-Systems. *J. Am. Chem. Soc.* **2015**, *137*, 7763−7768.

(15) Hu, Y.; Paterno, G. M.; Wang, X. Y.; Wang, X. C.; Guizzardi, M.; Chen, Q.; Schollmeyer, D.; Cao, X. Y.; Cerullo, G.; Scotognella, F.; Mullen, K.; Narita, A. pi-Extended Pyrene-Fused Double [7]Carbohelicene as a Chiral Polycyclic Aromatic Hydrocarbon. *J. Am. Chem. Soc.* **2019**, *141*, 12797−12803.

(16) Martin, M. M.; Hampel, F.; Jux, N. A Hexabenzocoronene-Based Helical Nanographene. *Chem. - Eur. J.* **2020**, *26*, 10210−10212.

(17) Castro-Fernandez, S.; Cruz, C. M.; Mariz, I. F. A.; Marquez, I. R.; Jimenez, V. G.; Palomino-Ruiz, L.; Cuerva, J. M.; Macoas, E.; Campana, A. G. Two-Photon Absorption Enhancement by the Inclusion of a Tropone Ring in Distorted Nanographene Ribbons. *Angew. Chem., Int. Ed.* **2020**, *59*, 7139−7145.

(18) Dusold, C.; Sharapa, D. I.; Hampel, F.; Hirsch, A. pi-Extended Diaza[7]helicenes by Hybridization of Naphthalene Diimides and Hexa-peri-hexabenzocoronenes. *Chem. - Eur. J.* **2021**, *27*, 2332−2341.

(19) Liu, B.; Bockmann, M.; Jiang, W.; Doltsinis, N. L.; Wang, Z. Perylene Diimide-Embedded Double [8]Helicenes. *J. Am. Chem. Soc.* **2020**, *142*, 7092−7099.

(20) Medel, M. A.; Tapia, R.; Blanco, V.; Miguel, D.; Morcillo, S. P.; Campana, A. G. Octagon-embedded carbohelicene as chiral motif for CPL emission of saddle-helix nanographenes. *Angew. Chem., Int. Ed.* **2021**, *60*, 6094−6100.

(21) Xu, F.; Yu, H.; Sadrzadeh, A.; Yakobson, B. I. Riemann Surfaces of Carbon as Graphene Nanosolenoids. *Nano Lett.* **2016**, *16*, 34−39.

(22) Naaman, R.; Waldeck, D. H. Chiral-Induced Spin Selectivity Effect. *J. Phys. Chem. Lett.* **2012**, *3*, 2178−2187.

(23) Kettner, M.; Maslyuk, V. V.; Nürenberg, D.; Seibel, J.; Gutierrez, R.; Cuniberti, G.; Ernst, K.-H.; Zacharias, H. Chirality-Dependent Electron Spin Filtering by Molecular Monolayers of Helicenes. *J. Phys. Chem. Lett.* **2018**, *9*, 2025−2030.

(24) Carr, R.; Evans, N. H.; Parker, D. Lanthanide complexes as chiral probes exploiting circularly polarized luminescence. *Chem. Soc. Rev.* **2012**, *41*, 7673−7686.

(25) Ma, W.; Xu, L.; Wang, L.; Xu, C.; Kuang, H. Chirality-Based Biosensors. *Adv. Funct. Mater.* **2019**, *29*, 1805512.

(26) Zhang, D. W.; Li, M.; Chen, C. F. Recent advances in circularly polarized electroluminescence based on organic light-emitting diodes. *Chem. Soc. Rev.* **2020**, *49*, 1331−1343.

(27) Xiao, X.; Pedersen, S. K.; Aranda, D.; Yang, J.; Wiscons, R. A.; Pittelkow, M.; Steigerwald, M. L.; Santoro, F.; Schuster, N. J.; Nuckolls, C. Chirality Amplified: Long, Discrete Helicene Nanoribbons. *J. Am. Chem. Soc.* **2021**, *143*, 983−991.

(28) Sota, S.; Asami, Y.; Satsuki, T.; Seiichi, F.; Masayuki, T.; Isobe, H. Chiral intertwined spirals and magnetic transition dipole moments dictated by cylinder helicity. *Proc. Natl. Acad. Sci. U. S. A.* **2019**, *116*, 5194−5195.

(29) Wade, J.; Brandt, J. R.; Reger, D.; Zinna, F.; Amsharov, K. Y.; Jux, N.; Andrews, D. L.; Fuchter, M. J. 500-Fold Amplification of Small Molecule Circularly Polarised Luminescence through Circularly Polarised FRET. *Angew. Chem.* **2021**, *133*, 224−229.

(30) Wang, X.-Y.; Yao, X.; Müllen, K. Polycyclic aromatic hydrocarbons in the graphene era. *Sci. China: Chem.* **2019**, *62*, 1099−1144.

(31) Qiu, Z.; Asako, S.; Hu, Y.; Ju, C. W.; Liu, T.; Rondin, L.; Schollmeyer, D.; Lauret, J. S.; Mullen, K.; Narita, A. Negatively Curved Nanographene with Heptagonal and [5]Helicene Units. *J. Am. Chem. Soc.* **2020**, *142*, 14814−14819.

(32) Milton, M.; Schuster, N. J.; Paley, D. W.; Hernandez Sanchez, R.; Ng, F.; Steigerwald, M. L.; Nuckolls, C. Defying strain in the synthesis of an electroactive bilayer helicene. *Chem. Sci.* **2019**, *10*, 1029−1034.

(33) Beurskens, P. T.; Beurskens, G.; van den Hark, T. E. M. Heptahelicene, C30H18. *Cryst. Struct. Commun.* **1976**, *5*, 241.

(34) Birks, J. B.; Birch, D. J. S.; Cordemans, E.; Vander Donckt, E. Fluorescence of the higher helicenes. *Chem. Phys. Lett.* **1976**, *43*, 33−36.

(35) Vander Donckt, E.; Nasielski, J.; Greenleaf, J. R.; Birks, J. B. Fluorescence of the Helicenes. *Chem. Phys. Lett.* **1968**, *2*, 409−410.

(36) Barroso, J.; Cabellos, J. L.; Pan, S.; Murillo, F.; Zarate, X.; Fernandez-Herrera, M. A.; Merino, G. Revisiting the racemization mechanism of helicenes. *Chem. Commun.* **2018**, *54*, 188−191.

(37) Sanchez-Carnerero, E. M.; Agarrabeitia, A. R.; Moreno, F.; Maroto, B. L.; Muller, G.; Ortiz, M. J.; de la Moya, S. Circularly Polarized Luminescence from Simple Organic Molecules. *Chem. - Eur. J.* **2015**, *21*, 13488−13500.

(38) Arrico, L.; Di Bari, L.; Zinna, F. Quantifying the overall efficiency of circularly polarized emitters. *Chem.—Eur. J.* **2020**, *26*, 1−16.

(39) Kiran, V.; Mathew, S. P.; Cohen, S. R.; Hernandez Delgado, I.; Lacour, J.; Naaman, R. Helicenes - A New Class of Organic Spin Filter. *Adv. Mater.* **2016**, *28*, 1957−1962.

(40) Naaman, R.; Paltiel, Y.; Waldeck, D. H. Chiral molecules and the electron spin. *Nat. Rev. Chem.* **2019**, *3*, 250−260.

(41) Naaman, R.; Waldeck, D. H. Spintronics and chirality: spin selectivity in electron transport through chiral molecules. *Annu. Rev. Phys. Chem.* **2015**, *66*, 263−281.